2014 IEEE/RSJ International Conference on
Intelligent Robots and Systems (IROS 2014)
September 14-18, 2014, Chicago, IL, USA

Towards Valve Turning using a Dual-Arm Aerial Manipulator

Christopher Korpela, Matko Orsag, and Paul Oh

Abstract— **We propose a framework for valve turning using an aerial vehicle endowed with dual multi-degree of freedom manipulators. A tightly integrated control scheme between the aircraft and manipulators is mandated for tasks requiring aircraft to environmental coupling. Feature detection is well-established for both ground and aerial vehicles and facilitates valve detection and arm tracking. Force feedback upon contact with the environment provides compliant motions in the presence of position error and coupling with the valve. We present recent results validating the valve turning framework using the proposed aircraft-arm system during flight tests.**

I. Introduction

Valve turning represents a classic controls problem along with insertion tasks and tool usage. The ground robotics community has largely solved these problems. There are many examples of door opening, using a drill, assembly of structures, and inserting a power plug by ground vehicles with one or more dexterous arms. Many of these tasks require position and/or force control and typical implementations involve force/torque sensing, vision systems, or a combination of these methods. The ground-based system must coordinate the vehicle and arm motions to perform these tasks. While the coupling between the environment (i.e. valve, knob, handle) and robot does influence the vehicle base with added contact forces/torques and friction, the base can typically maintain stability during the entire motion.

However, the strong coupling required during valve or knob turning greatly influences the dynamics of an aerial manipulator. Rigidity in the manipulator and the propagation of contact forces when interacting with the environment can cause crashes. There have been recent results where multi-DOF aerial manipulators have experienced coupling with the environment [1]–[4]. Other groups have investigated compliance in assembly tasks [5]–[7], or dynamic stability and control w.r.t. center of mass and moment of inertia variations [8]–[10].

Manuscript received June 21, 2014. This work was supported in part by the National Science Foundation (NSF) award CNS-1205490, Air Force Research Laboratory, under agreement number FA8655-13-1-3055, and the European Community Seventh Framework Program under grant No. 285939 (ACROSS). The U.S. Government is authorized to reproduce and distribute reprints for Governmental purposes not withstanding any copyright notation thereon. The views and conclusions contained herein are those of the authors and should not be interpreted as necessarily representing the official policies or endorsements, either expressed or implied, of the Air Force Research Laboratory, the U.S. Government, or the NSF.

C. Korpela and P. Oh are with the Drexel Autonomous Systems Lab, Drexel University, Philadelphia, PA 19104 USA cmk325@drexel.edu, paul@coe.drexel.edu

M. Orsag is with the Faculty of Electrical Engineering and Computing, University of Zagreb, 10000 Zagreb, Croatia morsag@fer.hr

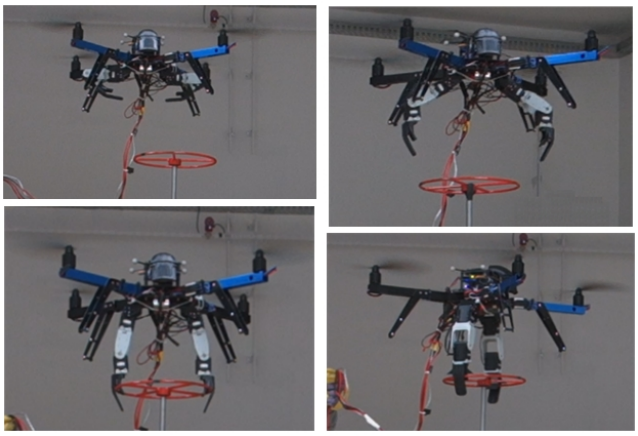

Fig. 1. MM-UAV dual-armed system in flight: approaching the valve, deploying arms, grabbing, and turning the valve.

This paper presents a solution to the valve turning problem from an aerial vehicle using dual 2-DOF manipulators, dubbed MM-UAV (Mobile Manipulating Unmanned Aerial Vehicle). A control scheme for the aircraft-arm system (Fig. 1) is implemented to allow for the strong coupling between the manipulators and environment. Sections II, III, and IV briefly describe the theory behind valve turning tasks and the algorithm used for detection. Sections V-VI details the kinematic and dynamic model for the aircraft and manipulators. The hardware and software components are found in Sec. VII. Section VIII presents validation results and flight tests.

II. The Valve Turning Problem

Valve, knob, and handle turning has been widely studied for use with industrial robots, mobile manipulators, and personal assistance robots. A typical requirement involves a grasp and turn of an object that remains fixed to the environment but allowed to rotate. Various techniques such as compliant motion, learning, passive compliance, hybrid position and force control, and impedance control have been implemented. All of these solutions deal with the challenges in the dynamic interaction of the manipulator with its environment.

Our framework and solution will be evaluated by performing valve turning, which is one of the tasks required for the recent DARPA Robotics Challenge (DRC) [11]. The task requires a robot to locate, approach, grasp, and turn an industrial valve with two hands. Valve turning presents a challenging test-case for any system due to the perception and dexterous manipulation required [12]. While a ground

robot can approach a value and easily become physically coupled to it, a flying robot with one or more manipulators faces far greater difficulties. The direct coupling between the manipulators and valve can cause sudden unexpected changes in the flight dynamics. The aerial manipulator must constantly adjust to compensate for the vehicle movement and further have adequate compliance to prevent a crash, particularly during the manipulator-environment coupling after grasping and while turning.

III. Valve Types and Features

Valves are found in virtually every industrial process including water and sewage processing, mining, power generation, processing of oil, gas and petroleum, food manufacturing, chemical and plastic manufacturing, and many other fields. Therefore, it is easy to imagine a disaster scenario where it is necessary to deploy an aerial robot to close a crucial valve and thus prevent further human casualties or damage. Unlike humanoid or mobile robots, closing a valve for an aerial robot is a highly complicated task which requires a robot to:

- Locate the handle
- Grab on to the handle
- Twist the handle, using the aircraft's own degrees of freedom

In industrial pipelines, different valves for gas, water, oxygen and many other gases and fluids are color coated. Although standards vary from country to country and industry to industry, some consistencies in standards have risen. In most cases, the following colors are assigned for use as both primary and secondary warnings [13]:

- Yellow - flammable materials
- Brown - toxic and poisonous materials
- Blue - anesthetics and harmful materials
- Green - oxidizing materials
- Gray - physically dangerous materials
- Red - fire protection materials

According to most standards, a good practice for piping systems which do not require warning colors is to paint them to differ from their surroundings. For humans, the use of these standards promotes safety and lessens chances of error in times of an emergency by providing a uniform color code to quickly warn personnel of outstanding hazards inherent in the materials involved. On the other hand, for robots, these standards insure an additional color filter layer in camera-based vision feedback algorithms. Given specific mission requirements (i.e. fire, pollution, or human safety), a robot can easily spot a specific valve using a color filter in order to separate it from its surroundings.

In practical applications, a single industrial pipeline system consists of various types of valves which could include butterfly valves, gate valves, ball valves, etc. No matter how the valve is mechanically designed, its handle is used to manually control the valve from outside its body. Automatically controlled valves often do not have handles, but some may have a handle in order to manually override the automatic control system in some disaster scenarios. Handles come in different shapes and sizes, with one of the most common shapes being the handwheel as seen in Fig. 2. The handwheel shape is ideally designed for the envisioned scenario: the aircraft grabs onto the valve handle and twists it using its own degrees of freedom. Although other shapes could be engaged as well because it is possible to land on them, they fall out of the scope of the proposed scenario.

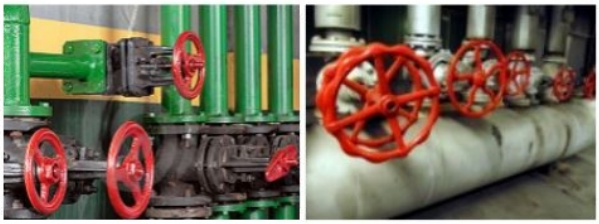

Fig. 2. Various industrial pipelines with handwheel valve handles.

There are two distinctive features of a handwheel handle design. The first concerns the circular shape of its outer rim that enables one to deploy some type of circle or ellipse detection algorithm. Varying in number from handle to handle are two, three, or more spokes that connect the circular rim with the handle hub. These spokes form lines that cross each other at the center of the handle, i.e. the hub. Using line detection algorithms, such as a Hough transform, it is possible to utilize this second distinctive handwheel feature.

IV. Valve detection algorithm

In this work we expand on the idea from [14]–[16], where the authors used various circular landmarks to localize an aerial vehicle. This technique is ideal for handwheel-shaped valve knobs due to their circular shape. Using the results from [17], one can use the data collected from the ellipse's shape in order to calculate the exact pose and position of the valve.

The idea behind the algorithm is to apply a 3-stage filter:

- 1st stage: Use color filtering based on different valve color specifications as described in Sec. III.
- 2nd stage: Search for ellipses on a binary image.
- 3rd stage: Search for lines within the ellipse to find spokes.

Reaching a desired threshold for spokes and the outer diameter of the valve, a good valve candidate is chosen. Detecting circular shapes of known radius R in 3D environments by observing their elliptic perspective projection has been tackled by many researchers in different applications [14]–[16]. The main approach used for this problem is based on projective linear transformation, namely collineation of a circle [17], by observing the camera with a pinhole model approach shown in Fig. 3. Because of the camera field of view (FOV) and in order to get a full view of the valve in all practical applications, it is necessary to place the camera outside the body center by $\vec{p}_C^B$ and rotate it by $\mathbf{R}_C^B$. It is this rotation that transforms a regular circular shape valve into

the projected ellipse. If the angle between the valve and the camera is $\frac{\pi}{2}$, then the image of the valve would be a perfect circle.

To detect ellipse parameters, the authors in [18] proposed an algorithm for direct least square fitting of ellipses. Through a simple mathematical transformation it is possible to write a well known 2D ellipse quadratic equation:

$$Ax^2 + 2Bxy + Cy^2 + 2Dx + 2Ey + F = 0,$$

as an oblique elliptical cone matrix equation [16]:

$$\begin{bmatrix} x & y & 1 \end{bmatrix} \mathbf{Q} \begin{bmatrix} x & y & 1 \end{bmatrix}^T = \mathbf{X} \begin{bmatrix} A & B & \frac{D}{f} \\ B & C & \frac{E}{f} \\ \frac{D}{f} & \frac{E}{f} & \frac{F}{f^2} \end{bmatrix} \mathbf{X}^T \quad (1)$$

where f stands for the focal length of the camera, and $A-F$ denote ellipse parameters. The authors in [17] proved that a circular object of known radius R, with normal $\vec{n}_V^C$ written in the camera frame, displaced from the center of the camera by vector distance $\vec{d}_V^C$, can be calculated using unit eigenvectors and eigenvalues, λ_1-λ_3 and λ_2-λ_3 respectively, of conic representation (1). This is accomplished using the following set of equations:

$$\vec{n}_V^C = S_1 \sqrt{\frac{\lambda_2 - \lambda_1}{\lambda_2 - \lambda_3}} \vec{v}_1 + S_2 \sqrt{\frac{\lambda_1 - \lambda_3}{\lambda_2 - \lambda_3}} \vec{v}_3 \quad (2)$$

$$\vec{d}_V^C = z_0 \left(S_1 \lambda_3 \sqrt{\frac{\lambda_2 - \lambda_1}{\lambda_2 - \lambda_3}} \vec{v}_1 + S_2 \lambda_2 \sqrt{\frac{\lambda_1 - \lambda_3}{\lambda_2 - \lambda_3}} \vec{v}_3 \right) \quad (3)$$

with z_0 being a radius dependent factor $z_0 = S_3 \frac{r}{\sqrt{-\lambda_2 \lambda_3}}$, and S_{1-3} undetermined signs. The signs can be determined by restraining ourselves to situations where $\vec{n}_V^C$ faces the camera and the valve itself is in front of the camera. For a conic to represent an ellipse, one of the eigenvalues must be less then zero. Therefore, the eigenvalues and corresponding eigenvectors are ordered in the following manner: $\lambda_3 < \lambda_2 \leq \lambda_1$. This analysis calculates only 5 degrees of freedom, neglecting only the yaw angle of the valve. Due to the fact that it is not important to know exactly the yaw angle of the valve in order to grasp it, this paper does not discuss how to calculate the yaw angle. However, the yaw angle could easily be calculated using the point where the valve spokes cross.

Once we know the position of the valve in the camera coordinate system, it is straightforward to calculate its position in the MM-UAV body frame, keeping in mind the rotation of the camera $\mathbf{R}_C^B$ and displacement from the body center $\vec{p}_C^B$:

$$\vec{d}_V^B = \vec{p}_C^B + \mathbf{R}_C^B \vec{d}_V^C \quad (4)$$

$$\vec{n}_V^B = \mathbf{R}_C^B \vec{n}_V^C \quad (5)$$

V. Modeling

Much of the previous work in quadrotor control assumes the geometric center and quadrotor center of mass are coincident. With the introduction of two manipulators used for valve turning, the center of mass shifts and the inertia properties change based on arm joint angles and environmental contact forces and torques.

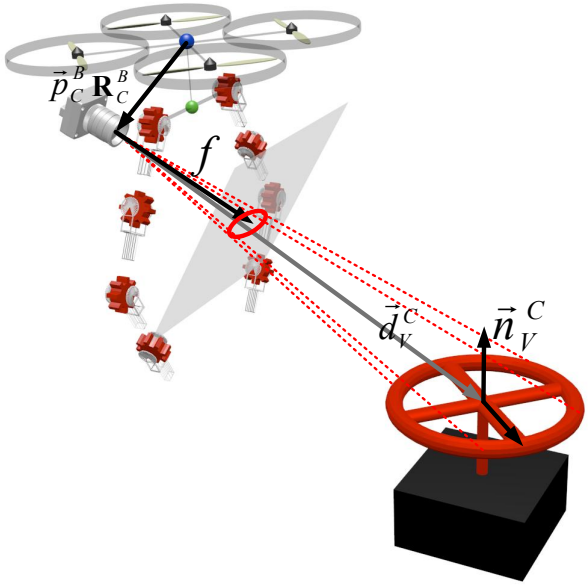

Fig. 3. Valve detection using a pinhole model camera displaced from the body center by $\vec{p}_B^C$ and rotated by $\mathbf{R}_B^C$. The image plane is shown in the focus of the camera. The figure shows how a circular object (i.e. valve) is projected onto an ellipse on the image plane.

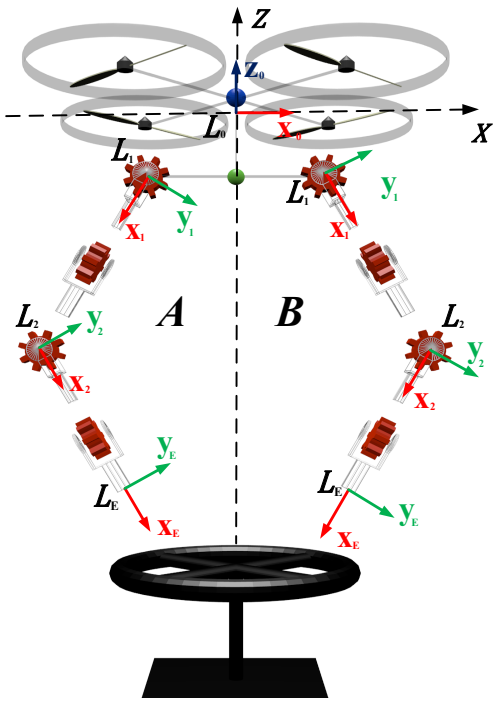

Fig. 4. Coordinate System (links expanded for clarity). 4 DOFs are shown for each arm to indicate a future arm design.

TABLE I
DENAVIT-HARTENBERG PARAMETERS FOR MANIPULATOR

Link Number	θ (rad.)	d (mm)	a (mm)	α (rad.)
1	q_1	0	L_1	0
2	q_2	0	L_2	0

A. Aircraft-Arm Kinematics

The coordinate system for the aircraft-arm system is shown in Fig. 4. The position and orientation of the body frame can be expressed in standard form as $p_b = [x\ y\ z]^T$ and $\phi_b = [\psi\ \theta\ \varphi]^T$ where the frames are right-handed with Z pointed upward. Attitude is denoted by the yaw-pitch-roll Euler angles in the body frame ($Z\,Y\,X$).

The manipulators (noted as arms A and B with links L_i) are symmetrical and attached below the center of gravity of the quadrotor frame and equally offset from the vehicle's geometric center. Forward kinematics for the two serial chain manipulators are derived using Denavit-Hartenberg (DH) parameters as shown in Table I. Parameters θ, d, a, and α are in standard DH convention and q_i for $i = 1$ to n are joint variables for the arm. The direct kinematics function relating the quadrotor body to the end-effector frame, p_e, is:

$$p_e = p_b + R_b p^b_{eb} \tag{6}$$

where p^b_{eb} is the position of the end-effector with respect to the body frame. A similar analysis is performed in [19].

B. Aircraft-Arm Dynamics

The equations of motion for the center of mass of the geometric center of the generalized 6-DOF vehicle have the standard Newton-Euler form [20]:

$$\vec{F} = m_Q \dot{\vec{v}} + \mathbf{\Omega} \times m_Q \vec{v} \tag{7a}$$

$$\vec{\tau} = \mathbf{I}\dot{\mathbf{\Omega}} + \Omega \times \mathbf{I}\mathbf{\Omega} \tag{7b}$$

where F represents the combination of propeller, aerodynamic, and gravitational forces with vehicle mass, m_Q, linear velocity, v, linear acceleration, $\dot{v}$, and rotational velocity, Ω. Torque, τ, is calculated from the inertia matrix, I, and the rotational velocity and acceleration, Ω and $\dot{\Omega}$ respectively. The torque and force produced from the quadrotor propellers have to be taken into account. The torque $\vec{\tau}^i$ has two components, one coming from the actual propeller drag Q, and the other due to the displacement of the propeller from the center of mass $\Delta\vec{\mathbf{o}}^i_{CM}(q_j)$. In an aerial manipulator system, the center of mass shifts as each joint (q_j) of the manipulator rotates and the torque becomes a nonlinear function of the manipulator joint angles:

$$\vec{\boldsymbol{F}}_q(u) = \sum_{i=1}^{4} \vec{\mathbf{F}}(u)^i \tag{8a}$$

$$\vec{\boldsymbol{\tau}}_q(u, q_j) = \sum_{i=1}^{4} \vec{\mathbf{Q}}(u)^i + \Delta\vec{\mathbf{o}}^i_{CM}(q_j) \times \vec{\mathbf{F}}(u)^i \tag{8b}$$

VI. COUPLING

We consider valve turning tasks to be strongly coupled events where the aerial manipulator must achieve contact forces and torques capable of turning a valve. In contrast, a pick and place or insertion task only requires a brief moment of loose coupling with the ground during the grasp or insertion. We investigate the coupling between the environment and the aircraft-arm system.

Once the aircraft-arm system has taken position over the valve and the geometric center of the valve has been detected, we can assume that the valve is constrained on a plane which is parallel the bottom plate of the quadrotor and that the quadrotor center of mass is positioned directly above the pivot of the valve. We assume that the valve is 'perfectly' balanced, that is the pivot of the valve represents the center of mass in the plane on which the valve turns. As the arms are symmetric and articulate equal and opposite of each other, the combined arms' center of mass shifts along the z-axis of the quadrotor geometric center. A constrained grab, when the quadrotor arms come into contact with the valve and clamp on, can be represented by the following:

$$CM_{total} = \frac{Q_{cm}m_Q + A_{cm}m_A + B_{cm}m_B + V_{cm}m_V}{m_Q + 2m_A + m_V} \tag{9}$$

where CM_{total} is the new center of mass of the quadrotor Q, duals arms A and B, and valve V coupled system with m mass and cm center of mass. Next, the inertial tensor $I^{arm}_{i=A,B}$ for each arm link is calculated as:

$$I^{arm}_i = \mathbf{R}^X_{GC}{}^T \begin{bmatrix} I_{xx} & 0 & 0 \\ 0 & I_{yy} & 0 \\ 0 & 0 & I_{zz} \end{bmatrix} \mathbf{R}^X_{GC} + m^{arm}_i \left[\mathbf{c}^i \cdot \mathbf{c}^i \mathbf{I} + \mathbf{c}^i \otimes \mathbf{c}^i\right] \tag{10}$$

with transformation matrix $\mathbf{R}^X_{GC}$ that transforms the moment of inertia into a geometric center coordinate system, and the expression in brackets encompasses outer and inner products of each link's center of mass vector w.r.t. the quadrotor body frame (i.e. parallel axis theorem). One has to note that there are two arms, and four arm links, with their respective masses (m^{arm}_i). As the geometric center of the valve is calculated and the z-axis of the aircraft-arm system is aligned, the inertia of the valve can simply be modeled as a hollow cylinder, $I^{valve} = m_V r^2_V$ where r_V is the valve radius. The total system inertia becomes:

$$I_{total} = I^{quad} + \sum_{i=1}^{i=4} I^{arm}_i + I^{valve} \tag{11}$$

Once the arm is clamped, we can assume that the valve handle is a free floating mass rotating about the z-axis, affected only by the resulting friction in the system, that is now rigidly attached to the quadrotor. In order to model the coupling with the valve, we denote the valve's mass as $m_V >> (m_Q + m_A + m_B)$, which brings the center of mass (9) at the point of contact between the arms and the valve.

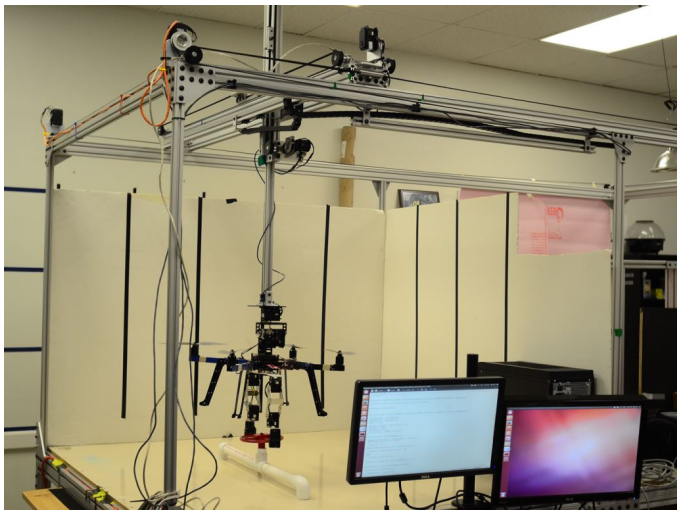

Fig. 5. Mini-SISTR with MM-UAV in a dual arm configuration.

VII. Hardware and Software Design

The aircraft-arm system is constructed using a quadrotor (3DRobotics), dual 2-DOF manipulators, and a standard webcamera. The vehicle contains the Arduino-based APM 2.6 autopilot with 880Kv brushless motors and 11 inch propellers. Power and communications are tethered providing for a greater payload capacity and fast messaging to the control station. The autopilot maintains a local control loop while the higher level processing is done off-board. The manipulators are assembled using off-the-shelf Dynamixel servo motors (MX-28), girders, brackets, and custom grippers. Final construction is shown in Fig. 1.

Software is integrated through a ROS infrastructure. Using the provided node based and message exchange system, it is easy to build the control system and establish communications between the aircraft and ground station. The mavlink protocol operates at 115k baud while the control loop runs at 30 Hz. Dynamixels use the controller package provided by ROS and the camera leverages OpenCV libraries.

VIII. System Validation and Flight Tests

To test and evaluate the valve turning framework, the system was implemented on a miniature gantry system [21] as shown in Fig. 5. A series of valve turning experiments were performed for model verification. The valve is plastic and scaled to an actual industrial valve with an outer diameter of 15 cm.

A. Validation Results

Fig. 6 shows the applied torques to the UAV yaw axis, right shoulder joint, right wrist joint, left shoulder joint, and left wrist joint of the two arms. When the arms make contact with the valve, the right and left shoulder joints experience the greatest applied torque throughout the turn. This is physically expected, due to the fact of the farther distance from the shoulder to the valve, and thus the applied torque has a higher value. Yaw torque values are the most crucial in the desired operation. Obviously, the larger the quadrotor,

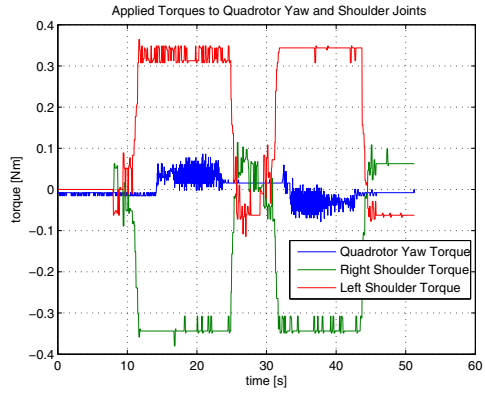

(a) Quadrotor yaw torque and shoulder roll joint torques for both arms [Nm] vs. [sec].

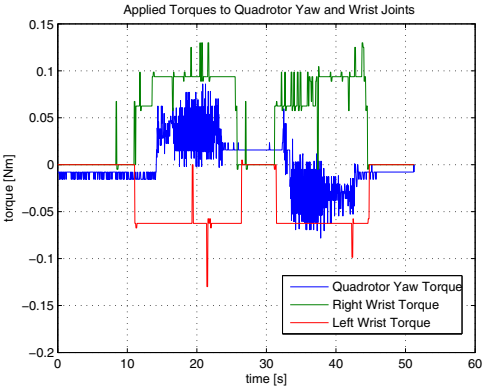

(b) Quadrotor yaw torque and wrist roll joint torques for both arms [Nm] vs. [sec].

Fig. 6. Applied torques during valve turning while attached to Mini-SISTR. The first grab and turn occurs between 10 and 25 seconds. The valve is released at time stamp 25 sec. and regrasped at time stamp 30 sec. for another rotation in the opposite direction.

the larger the torque it can apply on the valve. Therefore, the sole limitation of the operation is the amount of torque the quadrotor can produce. Given the size of the quadrotor, the moment of inertia of the valve can have various impacts on dynamics. The main drawback of this method is that due to the alignment of the quadrotor and valve yaw axis, the manipulator arms do not aid to the amount of torque applied to the valve.

B. Experimental Flight Tests

In addition to model verification, flight tests were performed to demonstrate and evaluate valve turning from a flying aircraft-arm system. Fig. 1 shows a series of snapshots during a valve turning flight experiment. Controller performance is shown in Fig. 7. Valve grabbing and turning occurs between time stamps 10 and 20 as shown in Fig. 7a. The strong coupling between the valve and manipulators is maintained during the entire turning sequence. Upon release by the grippers, the system increases in altitude and hovers above the target area. The arm joint torques and quadrotor yaw angle are analyzed during the turn.

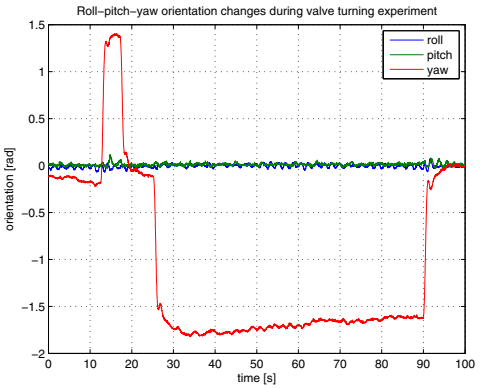

(a) Orientation control of aircraft.

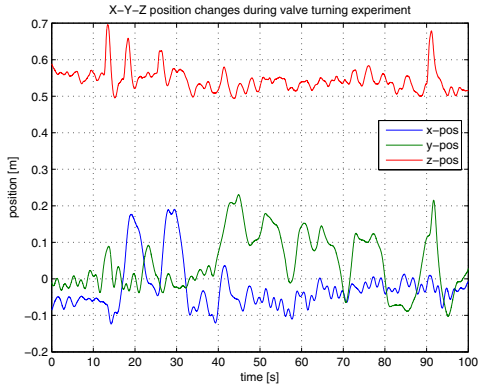

(b) Position control of aircraft.

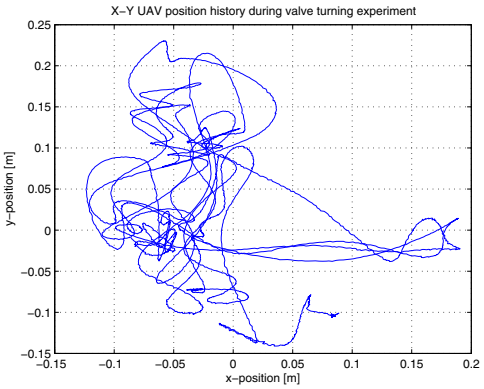

(c) X-Y position history during valve turning test.

Fig. 7. Control performance during valve turning test.

IX. Conclusions

In this paper an arm-aircraft system for valve turning is presented and validated using a gantry test rig. Our validation experiments confirm the kinematic and dynamic model and controller for the system. Test flights were conducted to evaluate the dual-armed configuration while turning a valve. Compliance control is paramount when using rigid manipulators to ensure aircraft stability. In the future, we plan to demonstrate our system on actual industrial valves with varying required torques.

References

[1] S. Kim, S. Choi, and H. J. Kim, "Aerial manipulation using a quadrotor with a two dof robotic arm," in *IEEE/RSJ International Conference on Intelligent Robots and Systems*, Tokyo, Japan, 2013.

[2] F. Huber, K. Kondak, K. Krieger, D. Sommer, M. Schwarzbach, M. Laiacker, I. Kossyk, S. Parusel, S. Haddadin, and A. Albu-Schaffer, "First analysis and experiments in aerial manipulation using fully actuated redundant robot arm," in *IEEE/RSJ International Conference on Intelligent Robots and Systems*, Tokyo, Japan, 2013.

[3] J. Scholten, M. Fumagalli, S. Stramigioli, and R. Carloni, "Interaction control of an uav endowed with a manipulator," in *Robotics and Automation (ICRA), 2013 IEEE International Conference on*, May 2013, pp. 4910–4915.

[4] M. Fumagalli, R. Naldi, A. Macchelli, R. Carloni, S. Stramigioli, and L. Marconi, "Modeling and control of a flying robot for contact inspection," in *Intelligent Robots and Systems (IROS), 2012 IEEE/RSJ International Conference on*, Oct 2012, pp. 3532–3537.

[5] K. Kondak, K. Krieger, A. Albu-Schaeffer, M. Schwarzbach, M. Laiacker, I. M. A. Rodriguez-Castano, and A. Ollero, "Closed-loop behavior of an autonomous helicopter equipped with a robotic arm for aerial manipulation tasks," in *International Journal of Advanced Robotic Systems*, 2013.

[6] A. Jimenez-Cano, J. Martin, G. Heredia, A. Ollero, and R. Cano, "Control of an aerial robot with multi-link arm for assembly tasks," in *Robotics and Automation (ICRA), 2013 IEEE International Conference on*, May 2013, pp. 4916–4921.

[7] V. Lippiello and F. Ruggiero, "Exploiting redundancy in cartesian impedance control of uavs equipped with a robotic arm," in *Intelligent Robots and Systems (IROS), 2012 IEEE/RSJ International Conference on*, 2012, pp. 3768–3773.

[8] I. Palunko and R. Fierro, "Adaptive feedback controller design and quadrotor modeling with dynamic changes of center of gravity," vol. 18, no. 1, August-September 2011, pp. 2626–2631.

[9] C. Korpela, M. Orsag, M. Pekala, and P. Oh, "Dynamic stability of a mobile manipulating unmanned aerial vehicle," in *Robotics and Automation (ICRA), 2013 IEEE International Conference on*, May 2013, pp. 4922–4927.

[10] M. Orsag, C. Korpela, and P. Oh, "Modeling and control of mm-uav: Mobile manipulating unmanned aerial vehicle," *Journal of Intelligent & Robotic Systems*, vol. 69, no. 1-4, pp. 227–240, 2013.

[11] [Online]. Available: http://www.theroboticschallenge.org/

[12] N. Alunni, C. Phillips-Grafftin, H. Suay, D. Lofaro, D. Berenson, S. Chernova, R. Lindeman, and P. Oh, "Toward a user-guided manipulation framework for high-dof robots with limited communication," in *Technologies for Practical Robot Applications (TePRA), 2013 IEEE International Conference on*, April 2013, pp. 1–6.

[13] MIL-STD-101B, "Military standard: Color code for pipelines and for compressed gas cylinders," [Online] Available: http://www.wbdg.org/, 1970.

[14] L. C. Mak and T. Furukawa, "A 6 DoF Visual Tracking System for a Miniature Helicopter," in *2nd International Conference on Sensing Technology*. IIST, Massey University, Nov. 2007, pp. 32–37.

[15] D. Eberli, D. Scaramuzza, S. Weiss, and R. Siegwart, "Vision based position control for mavs using one single circular landmark," *Journal of Intelligent and Robotic Systems*, pp. 495–512, 2011.

[16] S. Yang, S. Scherer, and A. Zell, "An onboard monocular vision system for autonomous takeoff, hovering and landing of a micro aerial vehicle," *Journal of Intelligent and Robotic Systems*, vol. 69, pp. 499–515, 2013.

[17] K. Kanatani and W. Liu, "3d interpretation of conics and orthogonality," *CVGIP: Image Underst.*, vol. 58, no. 3, pp. 286–301, Nov. 1993.

[18] A. Fitzgibbon, M. Pilu, and R. Fisher, "Direct least square fitting of ellipses," *Pattern Analysis and Machine Intelligence, IEEE Transactions on*, vol. 21, no. 5, pp. 476–480, 1999.

[19] G. Arleo, F. Caccavale, G. Muscio, and F. Pierri, "Control of quadrotor aerial vehicles equipped with a robotic arm," in *Control Automation (MED), 2013 21st Mediterranean Conference on*, 2013, pp. 1174–1180.

[20] S. Bouabdallah, P. Murrieri, and R. Siegwart, "Design and control of an indoor micro quadrotor," in *Proc. IEEE Int. Conf. Robotics and Automation ICRA '04*, vol. 5, 2004, pp. 4393–4398.

[21] C. Korpela, M. Orsag, and P. Oh, "Hardware-in-the-loop verification for mobile manipulating unmanned aerial vehicles," *Journal of Intelligent & Robotic Systems*, vol. 73, no. 1-4, pp. 725–736, 2014.